

Optical response features of Si-nanoparticle arraysAndrey B. Evlyukhin,^{1,2,*} Carsten Reinhardt,¹ Andreas Seidel,¹ Boris S. Luk'yanchuk,³ and Boris N. Chichkov¹¹*Laser Zentrum Hannover e.V., Hollerithallee 8, D-30419 Hannover, Germany*²*Kama State Academy of Engineering and Economics, 423810 Naberezhnye Chelny, Russia*³*Data Storage Institute (DSI), Agency for Science, Technology and Research, DSI Building, 5 Engineering Drive 1, 117608 Singapore, Singapore*

(Received 29 March 2010; published 8 July 2010)

Periodic structures of spherical silicon particles are analyzed using the coupled-dipole equations for studying optical response features and local electromagnetic fields. The model takes into account the electric and magnetic dipole moments of the particles embedded in a homogeneous dielectric medium. Particles with radius of 65 nm and larger are considered. It is shown that, due to the large permittivity of silicon, the first two Mie resonances are located in the region of visible light, where the absorption is small and the extinction is basically determined by scattering. The main contribution is given by the induced magnetic and electric dipoles of the particles. Thus, in contrast to metal particle arrays, here is a possibility to combine separately either the electric or magnetic dipole resonances of individual particles with the structural features. As a result, extinction spectra can have additional narrow resonant peaks connected with multiple light scattering by the magnetic dipoles and displaying a Fano-type resonant profile. Reflection and transmission properties of the Si particle arrays are investigated and the conditions of low light reflection and transmission by the particle arrays are discussed, as well as the applicability of the dipole approach. It is shown that the light transmission of finite-size arrays of Si particles can be significantly suppressed at the conditions of the particle magnetic dipole resonance. It is demonstrated that, using resonant conditions, one can separately control the enhancements of local electric and magnetic fields in the structures.

DOI: [10.1103/PhysRevB.82.045404](https://doi.org/10.1103/PhysRevB.82.045404)

PACS number(s): 78.20.Ci, 41.20.Jb, 42.30.Wb

I. INTRODUCTION

Optical properties of nanoparticle structures attract a lot of interest currently due to their application perspectives for controllable manipulation of optical fields on microscale and nanoscale levels. The combination of localized surface-plasmon resonances (LSPR) of individual metal particles and various particle structure configurations opens ways for the realization of important effects such as strong-field confinement and enhancement,¹⁻³ light energy guiding along nanoparticle chains,^{4,5} collective resonance response of periodic nanoparticle arrays,⁶⁻⁸ and surface-enhanced Raman spectroscopy with sensitivity down to a single molecule.^{9,10} Owing to the fact that optical response and local field distributions are strongly dependent on the particle shape and size,^{11,12} the interaction between particles,^{13,14} and the polarization of the incident light, it was suggested to get a strong magnetic response at visible-light frequencies using electromagnetically coupled pairs of gold nanoparticles.¹⁵⁻¹⁷ This effect, based on hybridization of individual nanoparticle modes,¹³ can be used for the creation of metamaterials with strong magnetic properties in optical frequency regions which are important for the realization of negative refraction and for the implementation of different micro-optical devices such as cavities, lenses, mirrors, and filters.¹⁸

Due to the Mie resonances of dielectric spheres with large permittivity values,¹⁹ dielectric particles also can be considered as basic elements of structures where the behavior of electromagnetic fields is controlled by particle and structural properties.²⁰ It has been shown that dielectric metamaterials constituted by polaritonic, nonmagnetic spheres can have negative effective permeability at infrared frequencies.^{21,22}

The strong magnetic response is connected to the existence of dielectric resonator (particle) modes for which the radial component of the magnetic field is not equal to zero.²³ In the Mie theory of dielectric scatterers the first spectral resonance from the side of large wavelengths always corresponds to the magnetic dipole term with the coefficient b_1 .¹⁹ In this case, a dielectric particle can be considered as a magnetic dipole scatterer of an incident electromagnetic wave at the resonant wavelength. This resonance results in an increased magnetic field in the near-field region around the particle. The concept and performance analysis of all-dielectric metamaterials, including their magnetic response, have recently been presented²⁴ and first experimental realizations were demonstrated.^{25,26} The enhancement of Raman scattering due to the resonant response of dielectric spheres has also been suggested.^{27,28}

Application of Mie scattering theory for studying the electrodynamic response of metal or dielectric particle structures embedded in a host material is widely used, beginning from the work of Lewin.²⁹ This theoretical approach allows an effective combination between the electric and magnetic polarizabilities obtained in Mie theory for an arbitrary sphere³⁰ and the coupled-dipole method. In this approximation, each particle is treated as a dipole scatterer and the total dipole moments of the particles are found by solving the coupled-dipole equations^{6,7,31-34} including the cases when particles are considered as electric and magnetic dipoles.³⁵⁻³⁷ It is necessary to note that the coupled-dipole approach can be applied if the distances between the particles in considered systems are larger than several particle radii.^{6,7} We will return to the question in the main part of the paper when the validity of the applied approximation will be discussed.

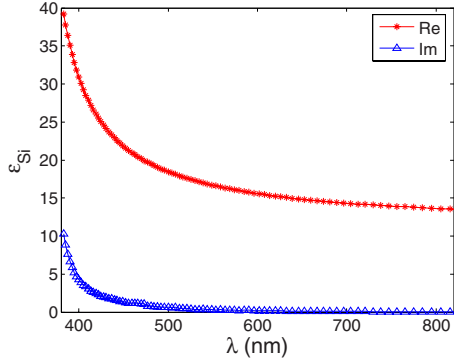


FIG. 1. (Color online) Dielectric permittivity of Si from Ref. 42.

In the framework of the coupled-dipole method, it was theoretically shown^{6,7,38,39} and experimentally confirmed^{8,40} that one-dimensional and two-dimensional (2D) periodic arrays of metal nanoparticles can have sharp spectral features in the optical response (additional resonant peaks in their extinction spectra) when the wavelength of the scattered light commensurate to the periodicity of the arrays and is in the same spectral range as the LSPR (for example, see a recent review given in Ref. 31). The width of the structural resonance, which is a result of multiple scattering of light, and its spectral position are controlled by the particle sizes, their distance, and their quantity in the array. In the limit of an infinite array, there is a possibility to obtain extremely narrow resonances for a certain ratio between the particle radius and the array period.^{7,31} The existence of narrow structural resonances in the extinction spectra of periodic metal particle systems determines their perspectives in chemical and biological sensor applications,⁴¹ and in surface-enhanced Raman spectroscopy.³⁸

In this paper, we theoretically study optical spectral features and local fields of alternative periodic two-dimensional structures consisting of spherical Si particles with diameters of 130 nm and larger under normal light incidence. It is shown that for such particles, due to the large permittivity of silicon (Fig. 1),⁴² the first two Mie resonances are located in the region of visible light, where the absorption is small and the extinction is basically determined by scattering with the main contribution given by the induced magnetic and electric dipoles. Thus, in contrast to metal particle arrays, here is a possibility to combine separately either the electric or magnetic dipole resonances of individual particles with structural features. Note that we consider the case of normal incidence of light, showing that the silicon particle structures have a set of original and interesting properties that would rather be expected for metal or magnetic particles. As a result, the extinction spectra can have additional narrow resonance peaks with the Fano-type shape^{43–45} connected with multiple light scattering by the magnetic dipoles. Moreover, using resonant conditions, one can control separately the enhancements of local electric and magnetic fields in the structures. We show that in the framework of the dipole approach, there exists a wavelength where the reflection of an infinite array, with a period smaller than the considered wavelength, is negligibly small due to interference between electric and mag-

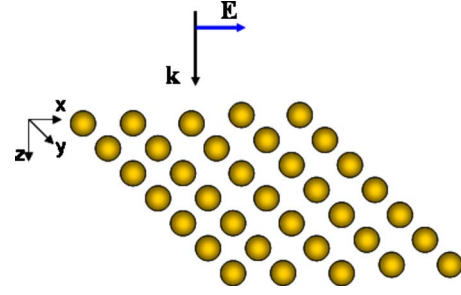


FIG. 2. (Color online) Schematic representation of physical system.

netic dipole scattering⁴⁶ which induces the electromagnetic transparency of the structure.

II. THEORETICAL BACKGROUND

We study the optical properties of a 2D rectangular particle array *embedded* in a homogeneous nonmagnetic transparent medium with a relative dielectric constant ϵ_d . The one-layer structure is located in the xy plane at $z=0$ with periodicity in the x and y directions. The particle array is irradiated by an external optical plane wave with electric and magnetic fields $\mathbf{E}^0(\mathbf{r})\exp(-i\omega t)=\mathbf{E}^0\exp(i\mathbf{k}_d\mathbf{r}-i\omega t)$ and $\mathbf{H}^0(\mathbf{r})\exp(-i\omega t)=\mathbf{H}^0\exp(i\mathbf{k}_d\mathbf{r}-i\omega t)$, respectively, see Fig. 2. The wave vector \mathbf{k}_d is given in the embedding dielectric medium with ϵ_d and ω is the circular frequency of the wave. In the following, the time dependence $\exp(-i\omega t)$ will be omitted.

In the dipole approximation, the particles are considered as electric and magnetic dipoles with electric and magnetic polarizabilities α^E and α^M , respectively. The corresponding electric and magnetic dipole moments \mathbf{p}_l and \mathbf{m}_l ($l=1,2,\dots,N$) can be found from the coupled-dipole equations written with the inclusion of the magnetic dipoles,^{36,47}

$$\mathbf{p}_l = \alpha^E \left[\mathbf{E}_l^0 + \frac{k_0^2}{\epsilon_0} \sum_{j \neq l}^N \left(\hat{G}_{lj} \mathbf{p}_j + \frac{i}{ck_0} [\mathbf{g}_{lj} \times \mathbf{m}_j] \right) \right],$$

$$\mathbf{m}_l = \alpha^M \left[\mathbf{H}_l^0 + k_0^2 \sum_{j \neq l}^N \left(\epsilon_d \hat{G}_{lj} \mathbf{m}_j - \frac{ic}{k_0} [\mathbf{g}_{lj} \times \mathbf{p}_j] \right) \right], \quad (1)$$

where $\mathbf{E}_l^0 \equiv \mathbf{E}^0(\mathbf{r}_l)$ and $\mathbf{H}_l^0 \equiv \mathbf{H}^0(\mathbf{r}_l)$ are the incident fields at the point of the particles with number l (under condition of normal incidence, which is considered in the paper, these fields are the same for all particles in the structures), k_0 is the wave number in vacuum, N is the total number of particles in the structure, $c=(\epsilon_0\mu_0)^{-1/2}$ is the vacuum speed of light (ϵ_0 and μ_0 are the vacuum permittivity and permeability, respectively), and i is the imaginary unit. The Green's tensor of the medium without particles is

$$\begin{aligned}\hat{G}_{lj} &\equiv \hat{G}(\mathbf{r}_l, \mathbf{r}_j) \\ &= \left[\left(\frac{1}{R_{lj}} + \frac{i}{k_d R_{lj}^2} - \frac{1}{k_d^2 R_{lj}^3} \right) \hat{U} \right. \\ &\quad \left. + \left(-\frac{1}{R_{lj}} - \frac{i3}{k_d R_{lj}^2} + \frac{3}{k_d^2 R_{lj}^3} \right) \mathbf{e}_R \mathbf{e}_R \right] \frac{e^{ik_d R_{lj}}}{4\pi},\end{aligned}\quad (2)$$

where $R_{lj} = |\mathbf{R}_{lj}| = |\mathbf{r}_l - \mathbf{r}_j|$, $\mathbf{e}_R \mathbf{e}_R$ is the dyadic constructed from the unit vector $\mathbf{e}_R = \mathbf{R}_{lj}/R_{lj}$, \hat{U} is the unit 3×3 tensor. The vector

$$\mathbf{g}_{lj} \equiv \mathbf{g}(\mathbf{r}_l, \mathbf{r}_j) = \frac{e^{ik_d R_{lj}}}{4\pi R_{lj}} \left(\frac{ik_d}{R_{lj}} - \frac{1}{R_{lj}^2} \right) \mathbf{R}_{lj} \quad (3)$$

is connected with the tensor (2) by the relationship

$$[\mathbf{g}(\mathbf{r}_l, \mathbf{r}_j) \times \mathbf{p}_j] = \nabla \times \hat{G}(\mathbf{r}_l, \mathbf{r}_j) \mathbf{p}_j,$$

here, the differentiation is carried out with respect to \mathbf{r}_l .

Note that the system of Eq. (1) can easily be obtained making use of the expressions for the electric \mathbf{E} and magnetic \mathbf{H} fields created by arbitrarily oriented electric \mathbf{p} and magnetic \mathbf{m} dipoles located at \mathbf{r}_p and \mathbf{r}_m , respectively,

$$\mathbf{E}^p(\mathbf{r}) = \frac{k_0^2}{\varepsilon_0} \hat{G}(\mathbf{r}, \mathbf{r}_p) \mathbf{p}, \quad \mathbf{H}^p(\mathbf{r}) = \frac{k_0 c}{i} \nabla \times \hat{G}(\mathbf{r}, \mathbf{r}_p) \mathbf{p},$$

$$\mathbf{H}^m(\mathbf{r}) = k_d^2 \hat{G}(\mathbf{r}, \mathbf{r}_m) \mathbf{m}, \quad \mathbf{E}^m(\mathbf{r}) = \frac{ik_0}{c\varepsilon_0} \nabla \times \hat{G}(\mathbf{r}, \mathbf{r}_m) \mathbf{m}.$$

The extinction cross section for a system of electric and magnetic dipoles can be obtained from the Maxwell equations,⁴⁸

$$\nabla \times \mathbf{E}(\mathbf{r}) = i\omega\mu_0 \left\{ \mathbf{H}(\mathbf{r}) + \sum_{j=1}^N \mathbf{m}_j \delta(\mathbf{r} - \mathbf{r}_j) \right\}, \quad (4)$$

$$\nabla \times \mathbf{H}(\mathbf{r}) = -i\omega \left\{ \varepsilon_0 \varepsilon_d \mathbf{E}(\mathbf{r}) + \sum_{j=1}^N \mathbf{p}_j \delta(\mathbf{r} - \mathbf{r}_j) \right\}. \quad (5)$$

From this system one obtains

$$\begin{aligned}\text{Re} \left\{ \int_{\Sigma} [\mathbf{E}^0(\mathbf{r}) \times \mathbf{H}^*(\mathbf{r})] ds + \int_{\Sigma} [\mathbf{E}(\mathbf{r}) \times \mathbf{H}^{0*}(\mathbf{r})] ds \right\} \\ = -\omega \text{Im} \sum_{j=1}^N [\mathbf{E}^{0*}(\mathbf{r}_j) \mathbf{p}_j + \mu_0 \mathbf{H}^{0*}(\mathbf{r}_j) \mathbf{m}_j].\end{aligned}\quad (6)$$

\mathbf{E}^0 and \mathbf{H}^0 are the electric and magnetic fields of the incident wave, e.g., the solution of Eqs. (4) and (5) without field sources and \mathbf{E} and \mathbf{H} are the scattered fields created by the dipoles. The surface integrals are taken over a closed surface Σ surrounding the dipoles. Using Eq. (6) the extinction cross section can be written in the form

$$\sigma_{ext} = \frac{k_d}{\varepsilon_0 \varepsilon_d |E_0|^2} \text{Im} \sum_{j=1}^N [\mathbf{E}^{0*}(\mathbf{r}_j) \mathbf{p}_j + \mu_0 \mathbf{H}^{0*}(\mathbf{r}_j) \mathbf{m}_j] \quad (7)$$

or

$$\sigma_{ext} = \sigma_{ext}^E + \sigma_{ext}^M \quad (8)$$

with $\sigma_{ext}^{E(M)}$ being the electric (magnetic) dipole part of the extinction cross section. The calculation of the scattering cross section for structures consisting of electric and magnetic dipole particles has been recently discussed in detail.³⁶

A. Infinite lattice

We first consider the general description of a plane electromagnetic wave interacting with an infinite 2D rectangular array of Si particles. Under normal incidence of an external plane wave at optical frequencies all particles will have the same electric and magnetic dipole moments \mathbf{p} and \mathbf{m} , respectively. Therefore, the system of Eq. (1) can be written as

$$\mathbf{p} = \alpha^E \left[\mathbf{E}^0 + \frac{k_0^2}{\varepsilon_0} \left(\hat{G}^0 \mathbf{p} + \frac{i}{ck_0} [\mathbf{g}^0 \times \mathbf{m}] \right) \right], \quad (9)$$

$$\mathbf{m} = \alpha^M \left[\mathbf{H}^0 + k_0^2 \left(\varepsilon_d \hat{G}^0 \mathbf{m} - \frac{ic}{k_0} [\mathbf{g}^0 \times \mathbf{p}] \right) \right], \quad (10)$$

where the electric \mathbf{E}^0 and magnetic \mathbf{H}^0 fields of the external wave are taken for $z=0$,

$$\hat{G}^0 = \sum_{j=1}^{\infty} \hat{G}_{0j}, \quad \mathbf{g}^0 = \sum_{j=1}^{\infty} \mathbf{g}_{0j}. \quad (11)$$

Due to periodicity in the x and y directions of an infinite particle array, $\mathbf{g}^0=0$ and the tensor \hat{G}^0 contains only the non-zero diagonal elements G_{xx}^0 , G_{yy}^0 , and G_{zz}^0 . Under these conditions, the connection between the electric and magnetic dipoles in Eqs. (9) and (10) disappears, and the quantities can be determined separately,

$$p_x = \frac{\varepsilon_0 E^0 \cos \varphi}{\varepsilon_0 / \alpha^E - k_0^2 G_{xx}^0}, \quad p_y = \frac{\varepsilon_0 E^0 \sin \varphi}{\varepsilon_0 / \alpha^E - k_0^2 G_{yy}^0}, \quad (12)$$

$$m_x = -\frac{H^0 \sin \varphi}{1/\alpha^M - k_d^2 G_{xx}^0}, \quad m_y = \frac{H^0 \cos \varphi}{1/\alpha^M - k_d^2 G_{yy}^0}, \quad (13)$$

where $H_0 = (\varepsilon_0 \varepsilon_d / \mu_0)^{1/2} E_0$ and φ is the angle between the external wave polarization and the x axis. A resonant response is obtained when the real part of any denominator in Eqs. (12) and (13) approaches zero. Let $\varphi=0$, then the electric dipole resonance will appear for

$$\text{Re}[\varepsilon_0 / \alpha^E - k_0^2 G_{xx}^0] = 0 \quad (14)$$

and the magnetic dipole resonance when

$$\text{Re}[1/\alpha^M - k_d^2 G_{yy}^0] = 0. \quad (15)$$

The conditions of the electric and magnetic resonances include different components of the tensor \hat{G}^0 depending on the array period along x and y directions. Note that only in the case of a square array $G_{xx}^0 = G_{yy}^0$.

In Sec. III. connections between the conditions (14) and (15) and the extinction spectra of the total structure will be derived. We will see that in addition to the resonances of individual particle [$\text{Re}(1/\alpha^E)=0$ and $\text{Re}(1/\alpha^M)=0$] further

resonances occur due to the diffraction coupling, i.e., the zeros of Eqs. (14) and (15). In contrast to previous works,^{6–8,31} additional resonances will appear due to the magnetic properties of particles.

An estimation of the reflection and transmission coefficients can be obtained when the total electric and magnetic fields are considered in the far zone for $z < 0$ and $z > 0$. Using the solutions (12) and (13) and considering the incident wave polarization along x axis ($\varphi=0$) the total electric field outside the array can be written as

$$\begin{aligned} E_x &= E^0 \left[e^{ik_d z} + \frac{k_0^2 G_{xx}^r}{\varepsilon_0 / \alpha^E - k_0^2 G_{xx}^0} - \frac{ik_d g_z^r}{1/\alpha^M - k_d^2 G_{yy}^0} \right], \\ E_y &= E^0 \frac{k_0^2 G_{yx}^r}{\varepsilon_0 / \alpha^E - k_0^2 G_{xx}^0}, \\ E_z &= E^0 \left[\frac{k_0^2 G_{zx}^r}{\varepsilon_0 / \alpha^E - k_0^2 G_{xx}^0} + \frac{ik_d g_x^r}{1/\alpha^M - k_d^2 G_{yy}^0} \right], \end{aligned} \quad (16)$$

where

$$\hat{G}^r = \sum_{j=1}^{\infty} \hat{G}(\mathbf{r}, \mathbf{r}_j), \quad \mathbf{g}^r = \sum_{j=1}^{\infty} \mathbf{g}(\mathbf{r}, \mathbf{r}_j). \quad (17)$$

Expressions for total magnetic field can be obtained similarly.

For the case of wavelength larger than the lattice period, both in x and y direction, one can write in the far-field approach (see Appendix),

$$G_{zx}^r = 0, \quad g_x^r = 0, \quad (18)$$

$$G_{xx}^r = \frac{i}{2S_L k_d} e^{\mp ik_d z}, \quad g_z^r = \frac{\pm 1}{2S_L} e^{\mp ik_d z}, \quad (19)$$

where S_L is the area of a lattice unit cell. The upper sign corresponds to $z < 0$ and the lower sign to $z > 0$. In this approach, the reflection and transmission coefficients for electric field are

$$r = \frac{ik_d}{2S_L} \left[\frac{1}{\varepsilon_0 \varepsilon_d / \alpha^E - k_d^2 G_{xx}^0} - \frac{1}{1/\alpha^M - k_d^2 G_{yy}^0} \right], \quad (20)$$

$$t = 1 + \frac{ik_d}{2S_L} \left[\frac{1}{\varepsilon_0 \varepsilon_d / \alpha^E - k_d^2 G_{xx}^0} + \frac{1}{1/\alpha^M - k_d^2 G_{yy}^0} \right], \quad (21)$$

respectively. For the intensity reflection one obtains

$$|r|^2 = \frac{k_d^2}{4S_L^2} ([\text{Re}(\alpha_{eff}^E) - \text{Re}(\alpha_{eff}^M)]^2 + [\text{Im}(\alpha_{eff}^E) - \text{Im}(\alpha_{eff}^M)]^2), \quad (22)$$

where we introduced for compactness the effective polarizabilities $\alpha_{eff}^E = 1/(\varepsilon_0 \varepsilon_d / \alpha^E - k_d^2 G_{xx}^0)$ and $\alpha_{eff}^M = 1/(1/\alpha^M - k_d^2 G_{yy}^0)$, which take into account interaction between the particles. We determine their electric and magnetic dipoles in the structure by the expressions,

$$p_x = \varepsilon_0 \varepsilon_d \alpha_{eff}^E E^0, \quad (23)$$

$$m_y = \alpha_{eff}^M H^0. \quad (24)$$

The intensity transmission is given by

$$\begin{aligned} |t|^2 &= \left[1 - \frac{k_d}{2S_L} [\text{Im}(\alpha_{eff}^E) + \text{Im}(\alpha_{eff}^M)] \right]^2 \\ &+ \frac{k_d^2}{4S_L^2} [\text{Re}(\alpha_{eff}^E) + \text{Re}(\alpha_{eff}^M)]^2. \end{aligned} \quad (25)$$

From the natural condition $|t|^2 + |r|^2 < 1$ one can obtain an estimation for the minimum distance between the nearest particles in the array when the dipole approximation breaks down. For validity of the dipole approximation the area of the lattice unit cell S_L must satisfy the self-consistent inequality

$$S_L^{1/2} > \sqrt{\frac{k_d}{2} \frac{|\alpha_{eff}^E|^2 + |\alpha_{eff}^M|^2}{\text{Im}(\alpha_{eff}^E) + \text{Im}(\alpha_{eff}^M)}}. \quad (26)$$

B. Finite-size lattice

In the case of a finite-size lattice, the system of Eqs. (1) has to be solved. Now, all components of the induced dipole moments differ from zero. The solution for the longitudinal components of a particle with number l can be written in the form

$$p_z^l = \alpha^E \frac{ik_0}{\varepsilon_0 c} \sum_{j=1, j \neq l}^N [\mathbf{g}_{lj} \times \mathbf{m}_j]_z, \quad (27)$$

$$m_z^l = -\alpha^M i c k_0 \sum_{j=1, j \neq l}^N [\mathbf{g}_{lj} \times \mathbf{p}_j]_z. \quad (28)$$

From these expressions it is obvious that the z components of the electric moments perpendicular to the lattice plane are determined by the electric field created by the magnetic dipoles and vice versa. The value of the z components and their distribution in the structures are depending on the wavelength, structure geometry, and particle number N . As will be shown in Sec. II, for the resonant wavelengths there is a noticeable increase in magnetic or electrical near fields with components perpendicular to the structure. Note, that in case of different periodicities in the x and y directions the electric and magnetic near fields can be controlled separately by the wavelength of the incident wave.

III. RESULTS AND DISCUSSIONS

Before going into a detailed discussion of the optical properties of periodic Si nanoparticle arrays let us first consider in Sec. III A the optical properties of single spherical Si particles. As a next step in Sec. III B, the response of infinite particle arrays is studied. The more realistic case of finite structures is addressed in Sec. III C. Since silicon is mostly covered with a native oxide layer also the nanoparticles should be considered as Si nanospheres with a thin shell of silicon oxide. The influence of such oxide shells of different thickness is studied in Sec. III D.

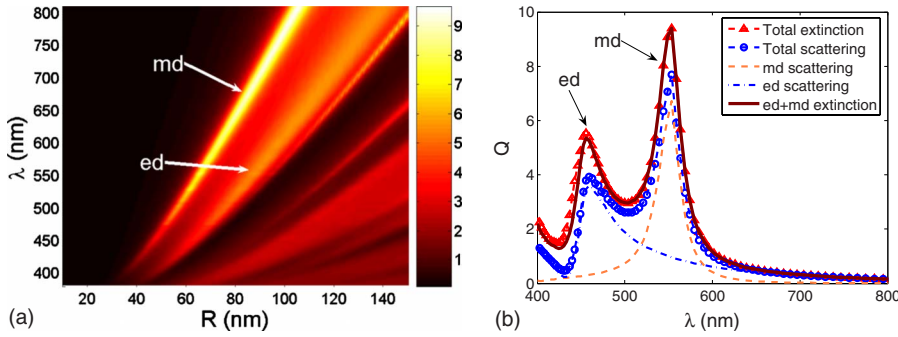


FIG. 3. (Color online) (a) Scattering efficiency spectra of Si spherical particles with the radius R located in air. (b) Extinction and scattering spectra of a Si particle ($R=65$ nm). The arrows indicate the electric dipole (ed) and magnetic dipole (md) contributions to the total efficiencies.

A. Optical response of single silicon particles

Particles with radii in the range of $R=40-100$ nm can have the first two Mie resonances located in the visible spectral region of light, see Fig. 3(a), where the scattering efficiency in air is given as a function of particle radius R and wavelength. In this case, the absorption is small and the extinction is basically defined by scattering with the main contributions generated by the induced magnetic and electric dipoles. The first two Mie resonances are determined by the expansion coefficients a_1 and b_1 , representing the contribution of the electric and magnetic dipole moments, respectively.⁴⁹ The Mie resonances, corresponding to the magnetic dipole (md) and to the electric dipole (ed) resonances, are indicated by the arrows in Fig. 3(a).

Figure 3(b) shows the extinction and scattering efficiencies calculated for Si nanospheres with $R=65$ nm. This specific particle radius provides the first two Mie resonances in the center of the visible spectrum and will thus be considered throughout the paper. To demonstrate the influences of the separate dipole moments on the total extinction and scattering efficiencies, these quantities are also calculated including only terms with the Mie scattering amplitudes a_1 and b_1 (dashed curves in Fig. 3).

Taking into account only the scattering amplitude a_1 , the extinction and scattering correspond to a pure electric dipole. Including only the term b_1 is equivalent to a pure magnetic dipole scatterer. The electric and magnetic polarizabilities of a sphere of arbitrary size and material can be obtained from the coefficients a_1 and b_1 of the Mie theory by the method described in Refs. 30 and 50. In this approach, the effective multipole polarizabilities may be found by dividing each multipole term of the scattered field by the corresponding partial-wave amplitude of the incident wave. For the electric and magnetic dipole polarizabilities one has

$$\alpha^E = i \frac{6\pi\epsilon_0\epsilon_d}{k_d^3} a_1, \quad \alpha^M = i \frac{6\pi}{k_d^3} b_1. \quad (29)$$

The dimensionless coefficients a_1 and b_1 are expressed by using the Riccati-Bessel functions with the arguments $k_d R$ and $k_p R$, with k_d and k_p being the complex wave numbers in the surrounding dielectric and in the particle, respectively.⁴⁹ The dimensions of the polarizabilities are determined by Eq. (1).

Note that the expressions, Eq. (29), have been obtained assuming the incidence of a plane wave. Using these polarizabilities for studying the optical response of particle arrays

requires therefore the distances between the particles to be larger than several particle diameters.⁷ The wavelength dependencies of the polarizabilities for Si particles with $R=65$ nm are shown in Fig. 4. The electric and magnetic dipole resonances in Fig. 3(b), i.e., the extinction maxima, coincide with the conditions $\text{Re}(\alpha^E)=0$ and $\text{Re}(\alpha^M)=0$. For simplicity and without loss of generality, we will consider in the following part of the paper the environment of the particle structures being air or vacuum, that is $\epsilon_d=1$.

B. Infinite arrays

The reflection and transmission properties of two-dimensional infinite Si particle arrays can be studied in the two limiting cases when first, the interparticle distances, i.e., the periods in the x and y directions are small compared to the incident wavelengths and second, when the array periods are equal or larger than incident wavelengths. We first consider the case of small periodicity. The polarization of the incident wave again is chosen along the x axis. The calculated reflectance $|r|^2$ and transmittance $|t|^2$ are presented in Fig. 5, showing a strong dependence on the incident wavelength. For the wavelengths corresponding to the single-particle resonances [cf. Fig. 3(b)] the transmission significantly decreases, especially for the magnetic resonance at $\lambda \approx 550$ nm, where only 10% of the incident energy is transmitted through the structure and the reflected energy increases up to 50%. The absorption also noticeably increases at the resonant conditions, see the curve marked with $R+T$ in Fig. 5. For large wavelengths outside the resonant region

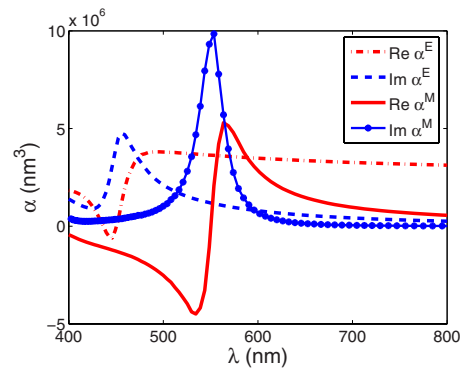


FIG. 4. (Color online) Electric α^E and magnetic α^M polarizabilities for a Si spherical particle of radius 65 nm located in air ($\epsilon_d=1$). Here the electric polarizability was divided by ϵ_0 .

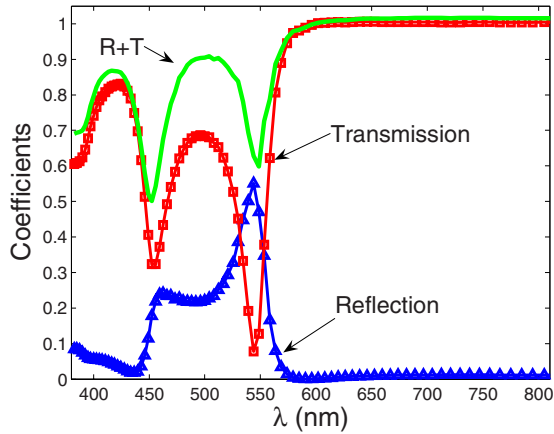


FIG. 5. (Color online) Reflectance and transmission spectra of infinite Si-particle structure, $R=65$ nm and $D=300$ nm.

almost all incident electromagnetic energy is transmitted through the array.

From the expression (22) one sees that the reflection becomes negligibly small if the effective electric and magnetic polarizabilities are equal to each other, including the real and imaginary parts. Indeed, the spectrum of the effective polarizabilities shown in Fig. 6 explicitly demonstrates that there is a wavelength when the electric and magnetic polarizabilities almost coincide, see the black arrows in Fig. 6. At this spectral position the reflection is negligibly small (Fig. 7). Note that if we consider increasing wavelengths the negligible reflection follows just after the reflection maximum, i.e., the reflection spectrum contains a sharp transition between the maximum and minimum reflection. This behavior is connected with coupling between the two scattering channels like physical systems with the Fano resonant responses when the interference of different excitation pathways can occur resulting in the effect of electromagnetically induced transparency.⁵¹ The position and width of this transition on the wavelength scale depends, in particular, on the particle size as it is demonstrated in Fig. 7 where particle radii of $R=55$ nm, $R=65$ nm, and $R=75$ nm have been considered.

Comparing the curves depicted in Figs. 4 and 6 it becomes clear that the radiative interaction between the particles in the structures with periods smaller than the incident wavelength only weakly perturbs the single-particle polariz-

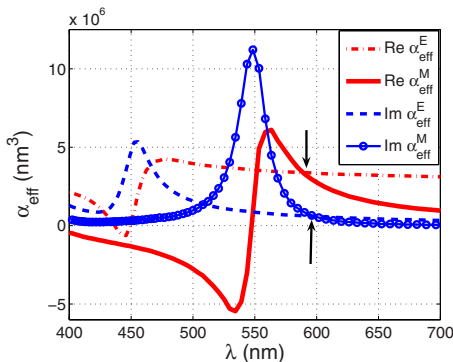


FIG. 6. (Color online) Effective polarizability spectra of infinite Si-particle structures, $D=300$ nm and $R=65$ nm.

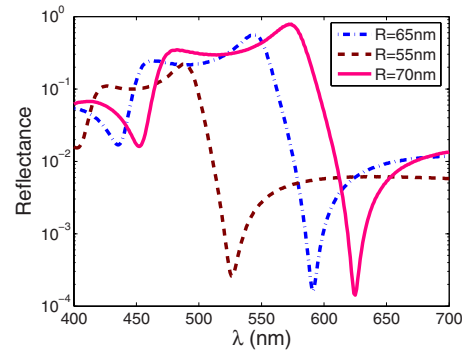


FIG. 7. (Color online) Reflection spectra of infinite Si-particle structures, $D=300$ nm.

abilities. So the scattering is determined by the scattering properties of the individual particles and the significant reduction in the reflection (Fig. 7) connects with the suppression of backward scattering by every particle in the structure.⁴⁶ It is also obvious that for wavelengths larger than the magnetic resonance, the real and imaginary parts of α_{eff}^M and the imaginary part of α_{eff}^E quickly become small compared to the real part of α_{eff}^E . Consequently, it would seem that in this spectral range the scattering process should be determined by the electric dipoles of the particles only. However, taking into account the inequality (26), there exists a boundary wavelength when this inequality is not fulfilled anymore and the dipole approach is inapplicable for wavelengths larger than the boundary. The boundary wavelength shifts to larger wavelengths with increasing array period (Fig. 8). For example, a structure with periodicity $D=200$ nm (dashed-dotted curve in Fig. 8) the boundary wavelength is equal to approximately 450 nm whereas for a structure with $D=300$ nm it is equal to 625 nm. Importantly, if the boundary wavelength is larger than the magnetic resonant wavelength the inaccuracy of the dipole approximation for large wavelengths is small, that is $|r|^2 + |t|^2 - 1 \ll 1$ (see Fig. 5 for $\lambda > 600$ nm).

As indicated in Sec. I, when the wavelengths of the scattered light are commensurate to the array periods in x and y directions and are in the spectral range of the individual particle resonances constituting the array, the extinction spectra can contain additional narrow resonant peaks due to the dif-

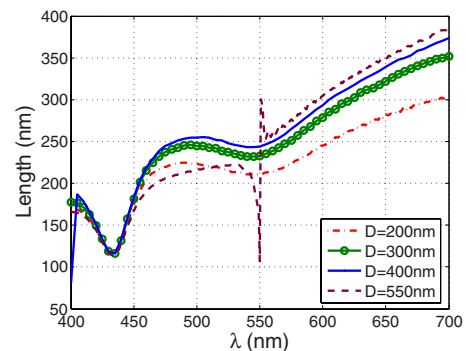


FIG. 8. (Color online) Wavelength dependence of the right-hand side part of the inequality (26) for infinite square arrays of Si particles, D is the array period ($D_L^{1/2}=D$), $R=65$ nm.

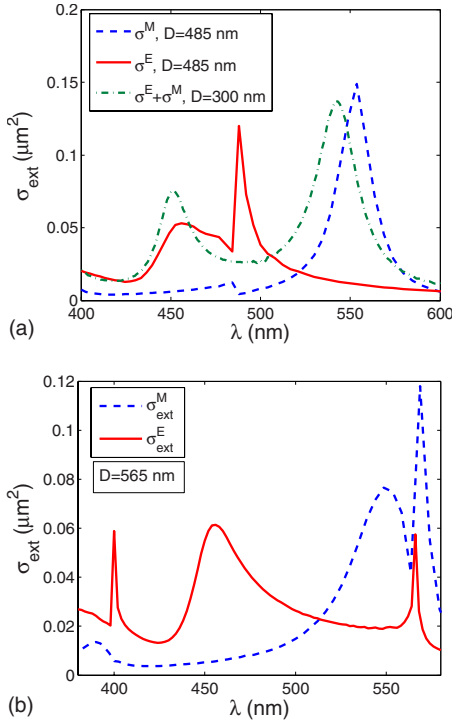


FIG. 9. (Color online) Extinction cross sections per one particle of infinite Si particle structures as a function of light wavelength. Period of the structure (a) $D=485$ nm and (b) $D=565$ nm, radius of the particles is 65 nm.

fraction coupling between the resonant particles. This is in analogy to the LSPR for metal particles^{8,40} and occurs in the same way in Si particle arrays with corresponding periodicity. Figure 9 shows the extinction cross sections per one particle calculated for Si particle arrays with periods of $D=485$ nm and $D=565$ nm. The particle radius is $R=65$ nm as before. The electric and magnetic dipole cross sections, Eq. (8), are plotted separately and compared with the total extinction cross section for the case $D=300$ nm, when no additional diffractive resonance appears. From Fig. 9(a) we see that the extinction spectrum contains additional narrow resonance corresponding only to the electric dipole response (σ_{ext}^E). The resonance is presented for the case when the period of the square array is smaller than the wavelength of the magnetic resonance but larger than that of the electric resonance. However, the magnetic resonance shows a red-shift compared with the case of small interparticle distance.

If the period of a structure is larger than the wavelength corresponding to the magnetic resonant response, the extinction spectrum will contain additional resonant peaks, including a peak corresponding only to the magnetic dipole resonance [Fig. 9(b)]. These additional peaks in the extinction curves are obtained when the resonant conditions (14) and (15) are realized. The detail analysis of the mechanisms of the effect can be found in Refs. 7 and 8. Here, we note that these resonances are connected with divergences of the terms G_{xx}^0 and G_{yy}^0 in Eqs. (14) and (15) as a function of wavelength for a fixed array period D , and also with the behavior of $\text{Re}(1/\alpha^E)$ and $\text{Re}(1/\alpha^M)$. The Fano-type asymmetric profiles of the additional resonances are the consequence of cou-

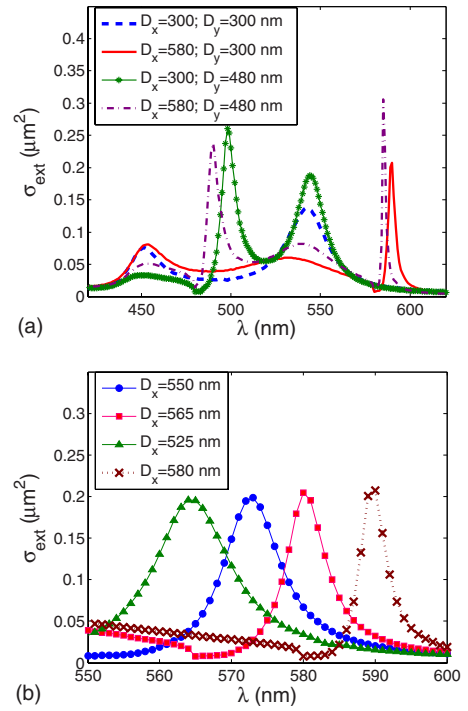


FIG. 10. (Color online) Extinction cross sections per one particle of infinite Si particle structures as a function of light wavelength. Radius of the particles is 65 nm. (a) Particle arrays with the different elementary cells ($D_x \times D_y$) and (b) particle arrays with fixed $D_y=300$ nm.

pling between individual particle scattering and multiple light scattering by all structure (see also Fig. 10).

The additional, diffractive resonances associated with the electric and magnetic dipoles can be excited independently due to the conditions (14) and (15) since G_{xx}^0 and G_{yy}^0 only coincide in case of arrays with a square elementary cell. If, in the general case, the lattice elementary cell is rectangular having different periodicities in x and y directions, the sums G_{xx}^0 and G_{yy}^0 will diverge at different wavelengths.

Thus, in order to controllably excite the additional, structural resonances associated with the electric and magnetic dipoles the interparticle distances in x and y directions that is perpendicular to the magnetic (electric) dipole orientation have to be adjusted. The polarization of the incoming wave is again set along the x axis. This possibility of controllable and selective excitation of electric and magnetic structural resonances is illustrated in Fig. 10(a), showing the extinction spectra of arrays with different elementary cells. For the case of a square array with $D_x=D_y=300$ nm only the resonances corresponding to the electric and magnetic dipole responses are visible. If only D_x is increased to 580 nm the additional resonance, i.e., the sharp peak at $\lambda \approx 590$ nm is associated with the magnetic dipole response. If the periodicity only in the y direction is increased, e.g., $D_y=480$ nm and $D_x=300$ nm, the additional peak at $\lambda \approx 550$ nm is associated with the electric dipole response. Increasing the elementary cell dimensions in both directions, $D_x=580$ nm and $D_y=480$ nm, we see two peaks associated with the electric and magnetic resonances [the dashed-dotted curve in Fig. 10(a)]. However, the positions of the peaks shift to the blue side in

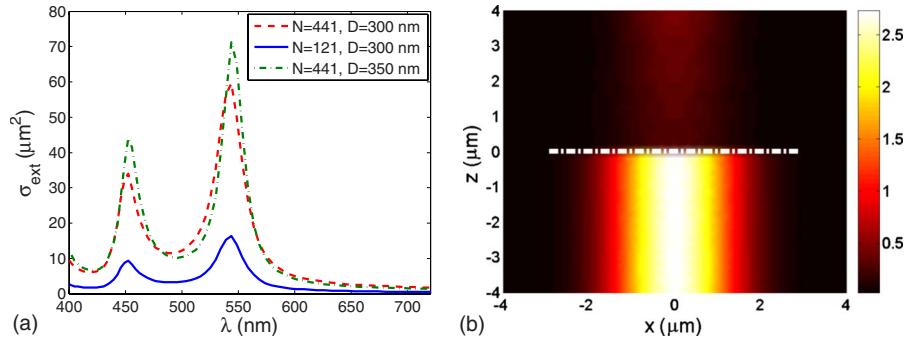


FIG. 11. (Color online) (a) Extinction cross-section spectra of 65 nm Si particles in two-dimensional square arrays of N particles. D is the particle spacing (smallest distance between the particles). (b) Electromagnetic energy distribution in the xz -plane ($y=0$) for the scattering of a light Gaussian beam $\lambda=548$ nm with dimension $4 \mu\text{m}$ by a finite square array of 65 nm Si particles (the white dashed-dotted line). Number of particles 441, the particle spacing $D=300$ nm.

comparison with the cases when only one additional resonance is excited.

Additionally, the values of the total extinction at the points of single-particle electric and magnetic resonances depend on D_x and D_y . For example, in the case of $D_x=300$ nm and $D_y=480$ nm, when only the diffractive resonance associated with the electric dipoles is realized, the extinction at the wavelength of the particle magnetic resonance noticeably increases, whereas the extinction at the point of the electric particle resonance decreases. For the case of $D_x=580$ and $D_y=300$ nm when the diffractive resonance associated with the magnetic dipoles is excited, we have the inverse situation. If the diffractive resonances associated with both dipoles can be excited the extinction values at the points of both, electric and magnetic dipole resonances of single particles decrease [Fig. 10(a)]. Notice that due to the divergence of the sums G_{xx}^0 and G_{yy}^0 , the extinction noticeably decreases for the wavelengths equaling to the array period in the corresponding direction [Fig. 10(a)].

Not only the position of the diffractive resonances depends on the particle periods but also the width of these resonances. If we consider particle arrays with increasing periods into the x direction but retaining the period into the y direction [Fig. 10(b)], we see that the diffractive resonance associated with the magnetic dipole shifts to the red side and gets narrow.

C. Finite-size arrays

In this section we discuss the properties of Si particle arrays consisting of a finite number of particles. As in the previous section we consider a linearly polarized light wave propagating in the positive z direction with polarization along the x axis. The extinction spectra for the cases, when the interparticle distance in a finite square array is smaller than the wavelength range under consideration, are shown in Fig. 11. As can be seen from the graphs, the two resonant peaks in Fig. 11(a) do not change their spectral positions with change in the particle spacing and particle number in the arrays, indicating that they correspond to the single-particle resonances, cf. Figs. 3(b) and 11(a). As in the case of infinite arrays the transmission through the finite arrays is

significantly decreased at the resonant wavelengths due to strong forward-directed scattering [Fig. 11(b)].

If the particle separation in finite arrays is larger than the wavelengths corresponding to the particle dipole resonances, the extinction spectra again show the additional diffractive peaks associated with the electric or magnetic particle dipoles. Analogously to the case of infinite arrays, by choosing separately the particle spacing in x and y directions one can obtain the diffractive resonances of the electric and magnetic types at different wavelengths, as demonstrated in Fig. 12. If the separation between the particles is small, the extinction spectrum exhibits only the particle dipole resonances, that is the curve corresponding $D_x=D_y=300$ nm in Fig. 12.

By increasing the spacing in x direction we can obtain the additional diffractive resonance associated with the particle magnetic dipole, occurring as a broad peak at $\lambda=590$ nm on the curve calculated for $D_x=580$ nm and $D_y=300$ nm in Fig. 12. Note that in this case the extinction at the particle magnetic resonance is decreased compared to the case of $D_x=D_y=300$ nm.

If the spacing is increased only in y direction, the diffractive resonance associated with the particle electric dipoles can be excited. The curve for $D_x=300$ nm and $D_y=480$ nm in Fig. 12 features an additional peak at $\lambda=550$ nm, corresponding to the diffractive electric dipole resonance. Importantly, the resonance value of the extinction

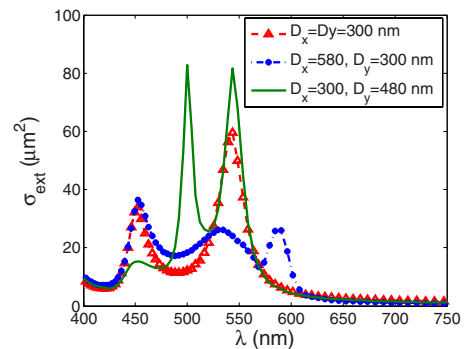


FIG. 12. (Color online) Extinction cross-section spectra of 65 nm Si particles in two-dimensional arrays of $21 \times 21=441$ particles. D_x , D_y are the particle spacings in the x and y directions, respectively.

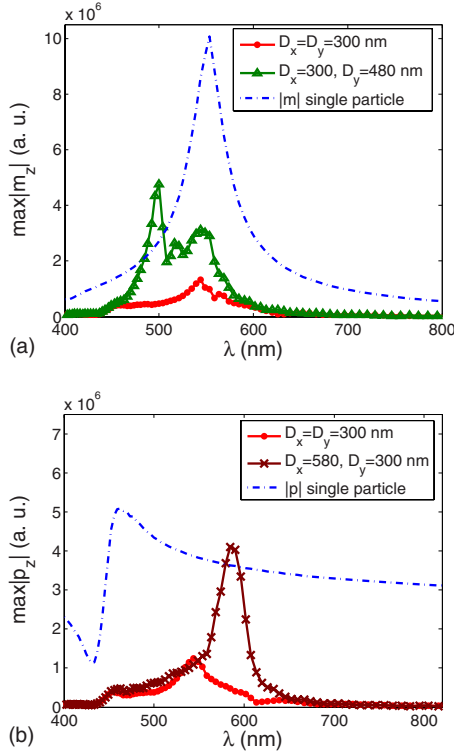


FIG. 13. (Color online) Maximal magnitude of longitudinal (a) magnetic m_z and (b) electric p_z dipole components in two-dimensional arrays of $21 \times 21 = 441$ particles. D_x, D_y are the particle spacings in the x and y directions, respectively. Radius of the particles is 65 nm.

for the particle magnetic resonance is also increased in this case.

Following the developed theoretical approach, the particle dipole moments in finite arrays should have nonzero longitudinal components perpendicular to the array plane. These components create longitudinal electromagnetic field in the near-field region, e.g., the electric dipoles generate the electric near field and the magnetic dipoles generate the magnetic near field. In resonance, the values of the components can significantly grow, hence increasing the intensity of the near fields. Note that the z components of magnetic dipoles are determined by the in-plane components of the electric dipoles and vice versa, Eqs. (27) and (28). Taking into account that the diffractive resonances associated with different dipoles can be excited independently, resulting in the resonant increase in particle electric or magnetic dipoles, we obtain the possibility to intensify the electric and magnetic near fields in the system by adjusting the corresponding parameters. Figure 13(a) demonstrates that the maximum of the magnetic dipole z components ($|m_z|$) distributed in an array of 441 particles noticeably increases at the wavelength corresponding to the diffractive resonance associated with electric dipole, visible as the sharp peak around 500 nm on the curve calculated for $D_x = 300$ nm and $D_y = 480$ nm in Fig. 13(a). This spectral position also corresponds to the diffractive peak on the curve with the same parameters as in Fig. 12. Moreover, the value of the z -component maximum is larger than the magnetic dipole of a single particle in free

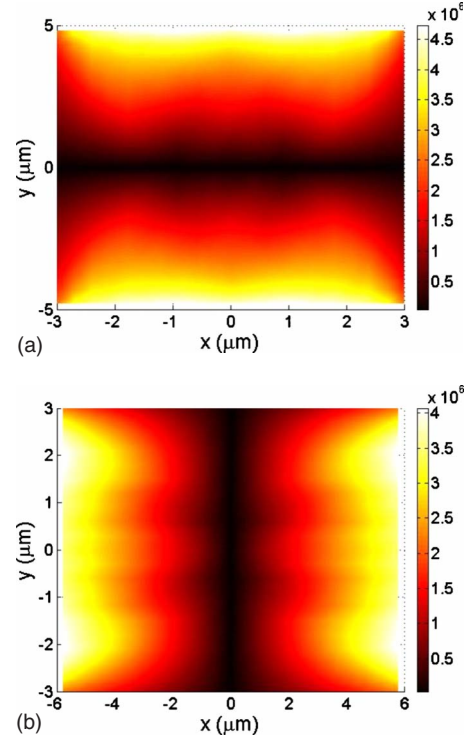


FIG. 14. (Color online) Distributions of z -component magnitudes of induced (a) magnetic and (b) electric dipoles (a.u.) in two-dimensional arrays of $21 \times 21 = 441$ particles. (a) $D_x = 300$ nm, $D_y = 480$ nm, λ corresponds to the global maximum of the curve in Fig. 13(a) with the same D_x, D_y . (b) $D_x = 580$ nm, $D_y = 300$ nm, λ corresponds to the global maximum of the curve in Fig. 13(b) with the same D_x, D_y .

space at the same wavelength [Fig. 13(a)]. For the system without diffractive resonances the values of m_z are small [the curve $D_x = D_y = 300$ nm in Fig. 13(a)].

This behavior is repeated for the electric dipole z component p_z but now the largest value of $|p_z|$ in the system corresponds to the diffractive resonance associated with the particle magnetic dipole [Fig. 13(b)]. The spatial distributions of magnetic and electric near fields in the Si particle arrays for the conditions of magnetic and electric diffractive resonances are shown in Figs. 14(a) and 14(b), respectively.

The creation of the strong longitudinal electric and magnetic near-field components arises as a boundary effect due to the finite size of the array. As a consequence, the maximum of the dipole longitudinal components is concentrated on the boundary of the structures. The maximum of $|m_z|$ originates at the array boundary parts being perpendicular to the electric polarization of incident waves. Correspondingly, the maximum of $|p_z|$ is reached on the array boundary parts which are perpendicular to the incident magnetic field polarization. Thus, changing the polarization of the incident light provides a unique possibility to change and control the near fields in the system on the subwavelength scale.

D. Influence of oxide shells

So far we considered pure silicon particles. However, in realistic experimental situations the particles are mostly cov-

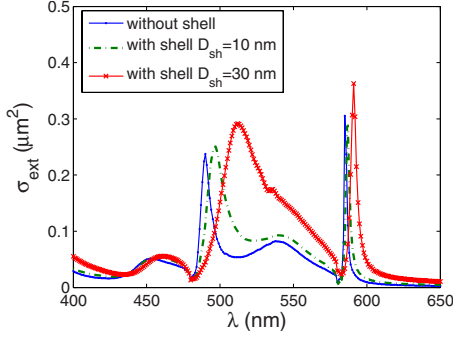


FIG. 15. (Color online) Extinction cross sections per one particle of infinite pure Si and Si+shell particle structures as a function of light wavelengths. Radius of the particles is 65 nm. $D_y = 480$ nm, $D_x = 580$ nm. Thicknesses of the shell are 10 and 30 nm, the shell dielectric constant 2.25.

ered by a thin dielectric layer of thermal silicon oxide of several nanometers thickness. Using the Mie theory for coated spheres,⁴⁹ we can apply the developed approach to study the optical response of particle arrays consisting of coated Si nanospheres. In the frame of the presented theoretical model, the coating can consist of an arbitrary material.

To study the influence of such dielectric shells on the optical response and especially to simulate the effect of the thermal oxide layer, we regard the role of thin dielectric shells with a dielectric constant of 2.25 in the extinction spectrum of such a shell-particle array. Figure 15 demonstrates the effect of shells with two different thicknesses of 10 and 30 nm on the extinction spectra in comparison to the case of uncoated spheres. For simplicity, we assume an infinite array consisting again of Si nanospheres with a radius of $R=65$ nm. The particle array under consideration has the periodicities of $D_x=580$ nm and $D_y=480$ nm in the x and y directions, respectively, showing the magnetic and electric diffractive resonances.

One can see that the dielectric shell influences predominantly the positions of the diffractive resonances. By increasing the thickness of the dielectric coating, the resonances are redshifted and broadened, whereas the influence of the shells on the magnetic dipole resonances is weaker than on the electric dipole ones. For relatively thin shells (10 nm and smaller), which could correspond to the natural oxide layers, the shell influence is weak for the both types of the resonances (Fig. 15). However, with increasing shell thickness the resonant shifts also increase and can be experimentally resolved.

As a result, the particle arrays provide a measurable sensitivity to the presence of even thin dielectric coatings due to the sharpness of the additional diffractive resonances. This effect could be used for creation of sensor devices on the base of the functionalized Si-particle structures with the ability to selectively bind certain molecules. The sensitivity of such a sensor device can be further enhanced when the electric and magnetic diffractive resonances are measured simultaneously.

IV. CONCLUSION

The coupled-dipole equation approach developed for arrays of electric and magnetic dipole particles has been ap-

plied to study the optical response of two-dimensional periodic structures of Si particles under the condition of normal light incidence. The applicability of the approach for different interparticle distances in the arrays was discussed. It was demonstrated that the optical response of a single spherical Si particle of certain dimensions can be considered as electromagnetic fields radiated by the induced electric and magnetic dipoles. The polarizabilities of the particles were determined by Mie theory. Infinite and finite particle arrays have been considered. The reflection and transmission spectra for the arrays with particle spacing, being smaller than the incident light wavelength, have been calculated and studied. The condition of negligibly small reflection (induced transparency) has been obtained. The possibility of strong suppression of light transmission through the finite-size particle arrays at the magnetic dipole resonance has been demonstrated. Moreover, it was found that the induction of the magnetic dipoles in the particles can result in additional diffractive magnetic-resonant peaks in the extinction spectra of the particle arrays when the distances between the particles are equal to the incident light wavelengths which in turn are larger than the resonant wavelengths for the electric and magnetic dipoles of single particles. The additional peaks had the Fano-type resonant profiles. It was shown that strong longitudinal electric and magnetic fields can be generated on the boundary of the finite-size Si-particle arrays at the diffractive resonances. It was found that the diffractive resonances of the particle arrays are noticeably shifted to the red spectrum direction if the particles are covered by a thin dielectric shell. The obtained results directly demonstrate that the Si-nanoparticle arrays have interesting and very important optical properties with the strong application potentials in nanophotonics and metamaterials.

ACKNOWLEDGMENTS

The authors acknowledge financial support of this work by the Schwerpunktprogramm SPP1391 “Ultrafast Nanooptics” of the Deutsche Forschungsgemeinschaft (DFG) and the Center for Quantum Engineering and Space-Time Research (QUEST).

APPENDIX: CALCULATION OF THE DIPOLE SUMS

Let us consider

$$G_{xx}^r = \sum_{j=1}^{\infty} G_{xx}(\mathbf{r}, \mathbf{r}_j), \quad g_z^r = \sum_{j=1}^{\infty} g_z(\mathbf{r}, \mathbf{r}_j) \quad (\text{A1})$$

in the far-field approximation.³¹ Using

$$G_{xx}(\mathbf{r}, \mathbf{r}') = \left[k_d^2 - \frac{\partial^2}{\partial x^2} \right] \frac{e^{ik_d|\mathbf{r}-\mathbf{r}'|}}{4\pi k_d^2 |\mathbf{r}-\mathbf{r}'|}, \quad (\text{A2})$$

$$g_z(\mathbf{r}, \mathbf{r}') = \frac{\partial}{\partial z} \frac{e^{ik_d|\mathbf{r}-\mathbf{r}'|}}{4\pi |\mathbf{r}-\mathbf{r}'|}, \quad (\text{A3})$$

and the Weil presentation of a spherical wave⁵²

$$\frac{e^{ik_d r}}{r} = \frac{i}{2\pi} \int_{-\infty}^{\infty} \frac{1}{w} e^{i(ux+vy+w|z|)} dudv, \quad (\text{A4})$$

where $w = \sqrt{k_d^2 - u^2 - v^2}$, one can write

$$G_{xx}^r = \frac{i}{8\pi^2 k_d^2} \sum_{j=1}^{\infty} \int_{-\infty}^{\infty} \frac{k_d^2 - u^2}{w} e^{i[\mathbf{K}(\mathbf{r}_{\parallel} - \mathbf{r}_{\parallel}^j) + w|z|]} dudv, \\ g_z^r = \frac{\pm 1}{8\pi^2} \sum_{j=1}^{\infty} \int_{-\infty}^{\infty} e^{i[\mathbf{K}(\mathbf{r}_{\parallel} - \mathbf{r}_{\parallel}^j) + w|z|]} dudv, \quad (\text{A5})$$

where $\mathbf{r}_{\parallel} = (x, y)$, $\mathbf{r}_{\parallel}^j = (x_j, y_j)$, and $\mathbf{K} = (u, v)$. In the expression for g_z^r (+) corresponds to $z < 0$ and (-) to $z > 0$. Transmitting to a sum over reciprocal-lattice vectors \mathbf{L} of the direct particle lattice by

$$\sum_{j=1}^{\infty} e^{-i(ux_j + vy_j)} = \frac{(2\pi)^2}{S_L} \sum_{\mathbf{L}} \delta(-\mathbf{K} - \mathbf{L}), \quad (\text{A6})$$

one obtains

$$G_{xx}^r = \frac{i}{2S_L k_d^2} \sum_{\mathbf{L}} \frac{k_d^2 - L_x^2}{\sqrt{k_d^2 - L^2}} e^{-i\mathbf{L}\mathbf{r}_{\parallel} + i\sqrt{k_d^2 - L^2}|z|}, \\ g_z^r = \frac{\pm 1}{2S_L} \sum_{\mathbf{L}} e^{-i\mathbf{L}\mathbf{r}_{\parallel} + i\sqrt{k_d^2 - L^2}|z|}. \quad (\text{A7})$$

If the wavelength in the medium with ε_d is larger than the lattice spacing D then the all terms of the sums, except the zero term $\mathbf{L}=0$, are evanescent. This means we have a far-field approximation,

$$G_{xx}^r \approx \frac{i}{2S_L k_d} e^{\mp ik_d z}, \\ g_z^r \approx \frac{\pm 1}{2S_L} e^{\mp ik_d z}, \quad (\text{A8})$$

the upper sign for negative z and the lower sign for positive z . In this approximation we also have

$$G_{zx}^r = 0, \quad g_x^r = 0. \quad (\text{A9})$$

*a.b.evlyukhin@daad-alumni.de

- ¹D. P. Fromm, A. Sundaramurthy, P. J. Schuck, G. Kino, and W. E. Moerner, *Nano Lett.* **4**, 957 (2004).
- ²P. Mühlischlegel, H.-J. Eisler, O. J. F. Martin, B. Hecht, and D. W. Pohl, *Science* **308**, 1607 (2005).
- ³D. A. Genov, A. K. Sarychev, V. M. Shalaev, and A. Wei, *Nano Lett.* **4**, 153 (2004).
- ⁴M. Quinten, A. Leitner, J. R. Krenn, and F. R. Aussenegg, *Opt. Lett.* **23**, 1331 (1998).
- ⁵S. A. Maier, P. G. Kik, H. A. Atwater, S. Meltzer, E. Harel, B. E. Koel, and A. A. G. Requicha, *Nature Mater.* **2**, 229 (2003).
- ⁶S. Zou, N. Janel, and G. C. Schatz, *J. Chem. Phys.* **120**, 10871 (2004).
- ⁷V. A. Markel, *J. Phys. B* **38**, L115 (2005).
- ⁸B. Auguie and W. L. Barnes, *Phys. Rev. Lett.* **101**, 143902 (2008).
- ⁹N. Féliđj, J. Aubard, G. Lévi, J. R. Krenn, A. Hohenau, G. Schider, A. Leitner, and F. R. Aussenegg, *Appl. Phys. Lett.* **82**, 3095 (2003).
- ¹⁰W. Zhang, X. Cui, B.-S. Yeo, T. Schmid, C. Hafner, and R. Zenobi, *Nano Lett.* **7**, 1401 (2007).
- ¹¹K. L. Kelly, E. Coronado, L. L. Zhao, and G. C. Schatz, *J. Phys. Chem. B* **107**, 668 (2003).
- ¹²F. Hao, C. L. Nehl, J. H. Hafner, and P. Nordlander, *Nano Lett.* **7**, 729 (2007).
- ¹³P. Nordlander, C. Oubre, E. Prodan, K. Li, and M. I. Stockman, *Nano Lett.* **4**, 899 (2004).
- ¹⁴R. de Waele, A. F. Koenderink, and A. Polman, *Nano Lett.* **7**, 2004 (2007).
- ¹⁵A. N. Grigorenko, A. K. Geim, H. F. Gleeson, Y. Zhang, A. A. Firsov, I. Y. Khrushchev, and J. Petrovic, *Nature (London)* **438**, 335 (2005).
- ¹⁶T. Pakizeh, M. S. Abrishamian, N. Granpayeh, A. Dmitriev, and M. Käll, *Opt. Express* **14**, 8240 (2006).
- ¹⁷Y. Ekinci, A. Christ, M. Agio, O. J. F. Martin, H. H. Solak, and J. F. Löffler, *Opt. Express* **16**, 13287 (2008).
- ¹⁸V. M. Shalaev, *Nat. Photonics* **1**, 41 (2007).
- ¹⁹H. C. van de Hulst, *Light Scattering by Small Particles* (Dover, New York, 1981).
- ²⁰Y. F. Lu, L. Zhang, W. D. Song, Y. W. Zheng, and B. S. Luk'yanchuk, *JETP Lett.* **72**, 457 (2000).
- ²¹M. S. Wheeler, J. S. Aitchison, and M. Mojahedi, *Phys. Rev. B* **72**, 193103 (2005).
- ²²V. Yannopoulos and A. Moroz, *J. Phys.: Condens. Matter* **17**, 3717 (2005).
- ²³L. A. Vanshtein, *Electromagnetic Waves*, 2nd ed. (Radio i Svyaz, Moscow, 1988) (in Russian).
- ²⁴A. Ahmadi and H. Mosallaei, *Phys. Rev. B* **77**, 045104 (2008).
- ²⁵J. A. Schuller, R. Zia, T. Taubner, and M. L. Brongersma, *Phys. Rev. Lett.* **99**, 107401 (2007).
- ²⁶B.-I. Popa and S. A. Cummer, *Phys. Rev. Lett.* **100**, 207401 (2008).
- ²⁷M. Inoue and K. Ohtaka, *J. Phys. Soc. Jpn.* **52**, 1457 (1983).
- ²⁸M. Inoue, *Pure Appl. Chem.* **59**, 1253 (1987).
- ²⁹L. Lewin, *Electr. Engineers — Part III: Radio and Communic. Engineer.* **94**, 65 (1947).
- ³⁰W. T. Doyle, *Phys. Rev. B* **39**, 9852 (1989).
- ³¹F. J. García de Abajo, *Rev. Mod. Phys.* **79**, 1267 (2007).
- ³²A. B. Evlyukhin, S. I. Bozhevolnyi, A. L. Stepanov, and J. R. Krenn, *Appl. Phys. B: Lasers Opt.* **84**, 29 (2006).
- ³³A. B. Evlyukhin, S. I. Bozhevolnyi, A. L. Stepanov, R. Kiyan, C. Reinhardt, S. Passinger, and B. N. Chichkov, *Opt. Express* **15**, 16667 (2007).
- ³⁴I. P. Radko, A. B. Evlyukhin, A. Boltasseva, and S. I. Bozhevolnyi, *Opt. Express* **16**, 3924 (2008).
- ³⁵G. W. Mulholland, C. Bohren, and K. A. Fuller, *Langmuir* **10**,

- 2533 (1994).
- ³⁶O. Merchiers, F. Moreno, F. González, and J. M. Saiz, *Phys. Rev. A* **76**, 043834 (2007).
- ³⁷B. García-Cámara, F. Moreno, F. González, and O. J. F. Martin, *Opt. Express* **18**, 10001 (2010).
- ³⁸K. T. Carron, W. Fluhr, M. Meier, A. Wokaun, and H. W. Lehmann, *J. Opt. Soc. Am. B* **3**, 430 (1986).
- ³⁹V. A. Markel, *J. Mod. Opt.* **40**, 2281 (1993).
- ⁴⁰B. Auguié and W. L. Barnes, *Opt. Lett.* **34**, 401 (2009).
- ⁴¹S. Zou and G. C. Schatz, *Nanotechnology* **17**, 2813 (2006).
- ⁴²E. Palik, *Handbook of Optical Constant of Solids* (Academic, San Diego, CA, 1985).
- ⁴³U. Fano, *Phys. Rev.* **124**, 1866 (1961).
- ⁴⁴F. Hao, Y. Sonnefraud, P. Van Dorpe, S. A. Maier, N. J. Halas, and P. Nordlander, *Nano Lett.* **8**, 3983 (2008).
- ⁴⁵G. Bachelier, I. Russier-Antoine, E. Benichou, C. Jonin, N. Del Fatti, F. Vallée, and P.-F. Brevet, *Phys. Rev. Lett.* **101**, 197401 (2008).
- ⁴⁶M. Kerker, D.-S. Wang, and C. L. Giles, *J. Opt. Soc. Am.* **73**, 765 (1983).
- ⁴⁷X. M. Bendaña and F. J. García de Abajo, *Opt. Express* **17**, 18826 (2009).
- ⁴⁸M. Born and E. Wolf, *Principles of Optics* (Pergamon, Oxford, 1970).
- ⁴⁹C. F. Bohren and D. R. Huffman, *Absorption and Scattering of Light by Small Particles* (Wiley, New York, 1983).
- ⁵⁰L. Jylhä, I. Kolmakov, S. Maslovski, and S. Tretyakov, *J. Appl. Phys.* **99**, 043102 (2006).
- ⁵¹N. Papisimakis and N. I. Zheludev, *Opt. Photonics News* **20**, 22 (2009).
- ⁵²L. Mandel and E. Wolf, *Optical Coherence and Quantum Optics* (Cambridge University Press, Cambridge, England, 1995).